

# Evapotranspiration saturation amplifies climate sensitivity of terrestrial water yield

Received: 15 June 2024

Eyal Rotenberg <sup>1</sup>✉, Fyodor Tatarinov<sup>1</sup>, Jonathan D. Muller <sup>1,2</sup> & Dan Yakir <sup>1</sup>✉

Accepted: 10 November 2025

Published online: 23 November 2025

 Check for updates

Predicted climate change over land indicates decreasing precipitation in many regions and increased flooding in others. Globally, over 60% of land precipitation is consumed by evapotranspiration (ET); the remainder, available as runoff, recharge, and for consumption, is termed water yield (WY). Using a global dataset, we show that ET from ecosystems reaches a ‘saturation’ limit of about  $480 \pm 210 \text{ mm yr}^{-1}$  across climates and biomes, well below the energy-based limit predicted by the Budyko equation. This inflexibility in ET increases the sensitivity of WY to precipitation variability, implying enhanced vulnerability to flooding in wet regions and an accelerated approach to the limits of ecosystem and societal sustainability in dry regions. Both effects are also supported by model-based projections. WY thus provides a more sensitive and integrative indicator of climate impacts on terrestrial water resources and associated risks for ecosystems and society.

Climate change is altering the global hydrological cycle, with significant implications for precipitation patterns (P), evapotranspiration (ET), and water availability<sup>1–3</sup>. Water availability—the surplus of precipitation after ET—governs runoff, aquifer recharge, and the water accessible for ecosystem services and society. Globally, about 63% of annual land precipitation is consumed by ET<sup>4,5</sup>, making the remainder, termed water yield (WY), a critical indicator of environmental and societal resilience to climate variability<sup>6–10</sup>:

$$\text{WY} = \text{P} - \text{ET}$$

where ET includes leaf transpiration, soil evaporation, and evaporation associated with canopy interception, and WY includes recharge to deeper soil layers and aquifers, runoff, and changes in soil water storage.

Understanding the controls on ET has often relied on frameworks such as the Budyko equation, which describes the balance between water supply (precipitation, P) and atmospheric demand (potential ET, PET) based on the relationship between the evaporative index (ET/P) and the dryness index (PET/P)<sup>10–12</sup>. These empirical relationships suggest that ET is constrained by water in dry regions and by energy in humid ones, implying that ET should increase with P or PET as long as moisture or energy are available. Water yield and its runoff component

have been extensively studied at the watershed and basin scales for decades<sup>13,14</sup>, typically using annual precipitation and runoff measurements in hydrologically closed catchments, where Budyko-type approaches have shown considerable potential.

However, at the ecosystem scale, ET has been increasingly measured directly at high spatial and temporal resolutions using eddy covariance (EC) methods, widely implemented across the global FLUXNET network<sup>14–18</sup>. These observations demonstrate that ET is highly regulated by a range of ecophysiological factors, beyond the physical assumptions of the Budyko framework.

In addition to precipitation and energy, ET is controlled by stomatal conductance, which responds dynamically to atmospheric conditions, such as vapor pressure deficit (VPD), as well as by hydraulic limitations in transporting water from soil to the canopy<sup>19–23</sup>. Ecosystem-scale ET is also influenced by canopy traits and energy dissipation mechanisms, including non-evaporative heat loss via sensible heat flux (H), at both canopy<sup>24–26</sup> and leaf scales<sup>27,28</sup>. Precipitation must also translate into plant-available soil moisture before contributing to ET, making soil properties and rainfall distribution, as well as soil evaporation important intermediaries. Rising atmospheric CO<sub>2</sub> levels further complicate this picture: although increased CO<sub>2</sub> can reduce stomatal conductance, it may be offset by increased leaf area and elevated VPD<sup>20,22,29–31</sup>. This biological regulation of ET reflects

<sup>1</sup>Earth and Planetary Sciences, The Weizmann Institute of Science, Rehovot, Israel. <sup>2</sup>School for Climate Studies, Stellenbosch University, Stellenbosch, South Africa. ✉ e-mail: [eyal.rotenberg@weizmann.ac.il](mailto:eyal.rotenberg@weizmann.ac.il); [dan.yakir@weizmann.ac.il](mailto:dan.yakir@weizmann.ac.il)

evolutionary trade-offs between carbon gain and water conservation, optimizing water-use efficiency ( $WUE = GPP/ET$ )<sup>32</sup>.

Consequently, while precipitation remains a foundational climate metric, WY provides an integrative measure that reflects both atmospheric forcing and ecosystem-level regulation at different time scales<sup>13,14,33</sup>. It captures the consequences of changes in ET resulting from both climatic and biological processes.

This framework is particularly relevant for understanding ecosystem sustainability. The threshold for viability is not when P reaches zero, but when WY falls to zero<sup>8,34</sup> (assuming that soil water storage serves as a limited, short-term buffer)<sup>35,36</sup>. In such conditions, all precipitation is consumed by ET, leaving no residual water for runoff, recharge, or buffering against drought. Repeated years of  $WY = 0$  increase the likelihood of vegetation mortality, biome shifts, and desertification, which in turn can generate feedbacks to the climate system<sup>34</sup>.

Here, we hypothesize that climate change will affect water yield more strongly than it affects precipitation itself, because when supply (water, energy) is available, ET remains relatively inflexible due to ecophysiological regulations. Using a global dataset of eddy covariance (EC) measurements, we assess the reliability of ET predictions derived from Budyko-type models. Our analysis reveals that actual ET exhibits an apparent “saturation”—a relatively fixed upper bound well below Budyko’s predicted values<sup>7</sup>. This observation challenges the assumption that ET continues to rise with increasing precipitation and energy supply. When ET remains relatively constant, changes in precipitation are more directly expressed as changes in WY (i.e.,  $WY = P - ET$ ), amplifying the sensitivity of water yield to climate variability<sup>3</sup>.

## Results & discussion

**Apparent evapotranspiration ‘saturation effect’:** Evapotranspiration values calculated from the Budyko equation (i.e., predicted ET values;  $ET_{pred}$ ) were compared with the corresponding values obtained from eddy covariance measurements (i.e., observed ET values;  $ET_{obs}$ ) at the FLUXNET sites used in this study (Fig. 1A). The comparison shows that, above an evapotranspiration threshold of ~500 mm, the observed evapotranspiration values are well below the Budyko predicted values. Our analysis, which was based on 1041 ET data years across 185 globally distributed sites, further indicates that observed evapotranspiration demonstrates an apparent saturation limit, with little variation across sites and year, of  $480 \pm 210$  mm compared with a precipitation range of about 3500 mm (Fig. 1B, S1). Only rarely (21 times in all the data years) did evapotranspiration in forest and in savanna ecosystems (in high

net radiation sites, mostly in the tropics) exceed 1000 mm. This apparent ‘saturation’ response (i.e., evapotranspiration outflux approaches a limit as precipitation influx continues to increase) is demonstrated in Fig. 1B using data across biomes and climates. Some decline in evapotranspiration with increasing precipitation was also observed in a few very wet forest sites, which is likely due to low temperatures and limited radiation. Some sites with limited data (MF, EBF) showed no dependence of evapotranspiration on precipitation (Fig. S1).

In all biome types, a close linkage between changes in evapotranspiration and changes in precipitation is only observed in the water-limiting range (at low precipitation values). At higher, non-limiting precipitation, evapotranspiration is not limited by the moisture supply side but by the available energy (mainly net radiation;  $R_n$ ). Nevertheless, the data across all biomes and climates do not support such an energy limitation (Fig. 1C, S2). The global slope of 0.42 observed for the flux of latent heat of evaporation ( $LE = \lambda \cdot ET$ ; where  $\lambda$  is the enthalpy of water vaporization) as a function of the ecosystem’s annual mean net radiation (Fig. 1C) indicates that most of the absorbed energy is not used for evaporation. Instead, the excess energy must be dissipated through other pathways, most likely dominated by sensible heat flux. Even in biomes for which the slope of the latent heat versus net radiation curve is higher, the slope remained well below the energy-limiting line (where  $LE = R_n$ ; Fig. S2).

The effect of interactions between supply (amount of precipitation and regime) and demand (mainly  $R_n$  and VPD) on evapotranspiration is associated with a range of physical and physiological factors that are often summarized in the widely used Penman-Monteith equation<sup>37</sup> or in the simplified form of the Priestley-Taylor equation<sup>38</sup>. However, based on these equations, evapotranspiration is expected to increase nearly linearly to at least ~1600 mm, and non-linearly to ~3000 mm, with increasing precipitation, net radiation, and vapor pressure deficit, which is not observed in the actual eddy covariance data (Figs. 1B, C, S3).

Similar results of conservative evapotranspiration response were observed when the influence of the mean annual air temperature (Fig. S4) or of annual mean water vapor pressure deficit (Fig. S5) were examined. For example, for ENF sites, an increase in the annual average temperature ( $T_a$ ) from 0° to 20° was associated with a corresponding increase in mean annual evapotranspiration of less than 100 mm (Fig. S4). Some effects of climatic conditions (P,  $R_n$ , and  $T_a$ , but not VPD<sup>39</sup>) on ET were clearly evident only for the savannas and shrubland

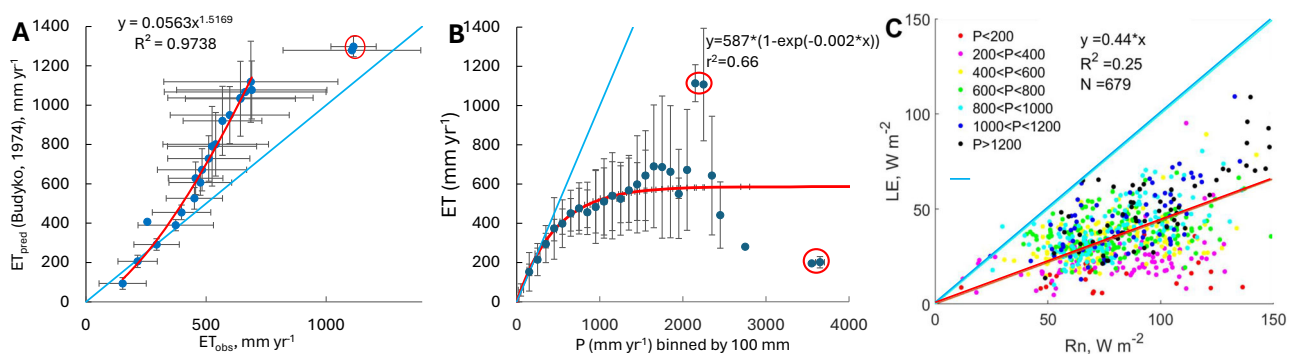


**Fig. 1 | Evapotranspiration saturation across ecosystems.** **A** Relationship across global FLUXNET sites between mean annual evapotranspiration ( $ET_{obs}$ ) and predicted annual evapotranspiration ( $ET_{pred}$ ), calculated using the Budyko equation with PET derived from the Priestley–Taylor method. Data are binned by 100 mm intervals of precipitation. Error bars indicate standard deviations; the blue line represents the 1:1 line. Data include 453 data years from 182 sites. Two sites marked by red circle (4 years) were excluded from regression. **B** Dependence of annual total observed ET on the measured annual precipitation (P) binned by 100 mm of

precipitation. Error bars represent standard deviations, the blue line is 1:1 line, a few outliers (representing 9 years out of 867 data years) were excluded from the regression (marked by red circles); and **C** dependence of annual mean latent heat flux ( $LE = \lambda \cdot ET_{obs}$ , where  $\lambda$  is the enthalpy of vaporization) on annual mean net radiation ( $R_n$ ), grouped by precipitation classes (in  $mm\ yr^{-1}$ ), using data from all biomes. N indicates the number of site-years available; differences in N reflect variation in data completeness across variables.

biomes, but these findings may reflect the low availability of data for those biomes.

**Mechanistic basis supporting ET saturation:** Our analysis reveals a robust saturation of ecosystem evapotranspiration (ET) at around  $480 \pm 210 \text{ mm yr}^{-1}$ , well below values predicted by Budyko-type energy- and supply-driven models. A key implication of this finding is that ET is not simply constrained by atmospheric drivers (precipitation or net radiation), but reflects also strong internal coupling to leaf physiology in general, and to gross primary production (GPP) in particular (Fig. S6).

A compelling explanation for this saturation emerges from the tight physiological coupling between transpiration and photosynthesis. At the leaf level, stomatal conductance regulates water vapor loss primarily to optimize carbon gain<sup>39,40</sup>. Photosynthesis, however, saturates under moderate to high radiation due to biochemical limits on carboxylation, electron transport, and triose phosphate utilization<sup>41,42</sup>. Once photosynthetic demand is met, stomatal aperture no longer increases with light, thereby limiting transpiration even when radiation and vapor pressure deficit (VPD) rise further<sup>22</sup>. Similarly, pigment light saturation imposes physical limits on the use of absorbed radiation for photochemistry. When pigment systems are saturated, excess energy is increasingly dissipated as sensible heat flux (H), as observed in our global evaluation of the Bowen ratio ( $\beta = 1.1 \pm 0.6$ ) and evaporative fraction (EF = 0.47; Fig. S7). This is consistent with independent reports<sup>18,43</sup>. Effective heat dissipation via the so-called ‘convective effect’ also highlights the significant reliance on sensible heat, in tandem with evapotranspiration, to achieve heat dissipation and temperature control at both the canopy<sup>24–26</sup> and the leaf scales<sup>27,28</sup>.

This interpretation is further supported by global patterns of water use efficiency (WUE = GPP/ET), which provide a direct measure of the carbon–water coupling. Multiple datasets show that WUE is relatively stable across climates and converges toward biome-specific optima, reflecting the optimization of stomatal behavior<sup>32,44–46</sup>. For example (Xue et al., 2015) demonstrate that WUE tends to plateau once leaf area index (LAI) exceeds  $\sim 2 \text{ m}^2 \text{ m}^{-2}$ , incoming solar radiation exceeds  $\sim 140 \text{ W m}^{-2}$ , and is insensitive to annual scale precipitation, indicating that canopy photosynthetic capacity constrains further increases in both GPP and ET. Recent ECOSTRESS-based global analyses confirm that plant functional types converge on narrow ranges of WUE despite diverse climates, underscoring biological regulation rather than environmental supply as the dominant control<sup>46</sup>. Our observational data-set clearly confirms this perspective, demonstrating a strong link between ET and GPP and a clear GPP-like saturation behavior (Fig. S6).

Thus, ET saturation can be viewed as an emergent property of constrained WUE. Because plants maintain a relatively stable ratio of carbon gain to water loss, ET cannot independently track increases in water or energy availability. Instead, optimization of carbon–water exchange, and biophysical limits on energy partitioning jointly constrain ET.

We also considered alternative possibilities, such as related to measurement uncertainty in eddy-covariance flux data. A primary concern is the energy balance closure (EBC) gap, which persists at most FLUXNET sites. Mauder et al. (2020; 2024)<sup>47,48</sup> show that the typical EBC ratio is  $\sim -0.85$  (i.e., a global mean shortfall of  $\sim 15\%$  between available energy and the sum of latent and sensible heat fluxes). Importantly, their analysis shows that EBC is relatively narrow across sites, and that this under-closure is primarily due to underestimation of sensible heat flux (H) rather than latent heat (LE), which directly governs evapotranspiration. Even under the extreme assumption that the entire missing energy were due to underestimated LE, the ET saturation threshold would rise from  $\sim 480 \text{ mm yr}^{-1}$  to at most  $\sim 550 \text{ mm yr}^{-1}$ , a minor adjustment that does not alter our interpretation. Furthermore, the saturation trend persists across sites with both high and low closure, and across both AmeriFlux and ICOS networks.

Thus, uncertainty in energy balance partitioning is unlikely to account for the consistent and physiologically interpretable patterns in ET behavior we observe globally.

We note, however, that this mechanistic interpretation should be viewed as a hypothesis rather than a definitive explanation. Other factors, such as soil moisture limitations, hydraulic constraints, or boundary-layer feedbacks, may also contribute to ET saturation in different contexts. While WUE provides a compelling unifying framework, more research is clearly needed to disentangle the relative contributions of these processes. A full mechanistic resolution lies beyond the scope of the present study but represents an important direction for future work.

**Sensitivity of water yield to precipitation amount:** In contrast to the saturation patterns evident for evapotranspiration (ET), water yield (WY) responds approximately linearly to precipitation (P) across the full precipitation range at the biome scale ( $R^2 > 0.8$  in most cases; Fig. 2). Grasslands exhibit lower slopes than forests, likely due to faster adjustments of total leaf area to changes in precipitation<sup>49</sup>.

This linearity reveals a striking sensitivity of WY to changes in P. For example, a  $\sim 40\%$  decline in precipitation (from  $\sim 700$  to  $\sim 400 \text{ mm}$ , within the range projected under climate change scenarios<sup>12</sup>) would cause nearly a 100% reduction in WY—essentially eliminating any flow of water beyond ET, in the absence of any ecosystem or land cover adjustments. In other words, relative changes in WY are much larger than the underlying changes in P. This amplification is most acute under dry conditions, where WY is already close to zero, emphasizing the vulnerability of ecosystems to drought and mortality. Vegetation responses to such stress—including tree mortality, reduced stand density, or transitions to grasses—can reduce ET and eventually restore positive WY, but often at the cost of biodiversity, carbon storage, and ecosystem services<sup>49</sup>.

The concept of  $P_{\text{WY}=0}$ , the precipitation threshold for zero WY (the x-intercept in WY–P relationships), provides further insight. Globally,  $P_{\text{WY}=0}$  averages  $371 \pm 88 \text{ mm}$  (Fig. 2, Table S1), a value consistent with the ET saturation point of  $480 \pm 210 \text{ mm}$  noted above. These thresholds likely reflect local adjustments in biome type, stand density, and leaf area<sup>12,50,51</sup>. Importantly,  $P_{\text{WY}=0}$  defines the limit of ecosystem sustainability: when precipitation balances ET on average, ecosystems cannot persist indefinitely, since soil moisture carry-over buffers water deficits for only 1–2 years<sup>17</sup>. Indeed, analyses of inter-annual means of P and ET at sites with  $\geq 3$  years of data show only one case where  $\text{ET} > \text{P}$ , and none when  $\geq 5$  years are considered. While shallow groundwater can locally support ET, its influence is limited to 22–32% of the global land area<sup>52</sup> and does not alter the global WY–P relationship. Thus, while WY does not replace P or ET as a metric to assess climate change, it offers a clear advantage in this context: it integrates inputs and losses while magnifying their combined effects.

Notably, our observationally-based results demonstrating enhanced sensitivity of water yield to changes in precipitation are also observed in the widely used coupled model intercomparison project (CMIP6) future projections. We obtained mean outputs for annual precipitation and evaporation (E) over land from 27 CMIP6 models<sup>53</sup> (see ‘‘Methods’’) to examine the relative changes in the water yield (termed here  $\text{WY}_{\text{P-E}}$ ) between the end of the 20th and the end of the 21st centuries (1980–1999 compared with 2080–2099, using the SSP5-8.5 scenario) (Fig. 3).

It is important to note that vegetation responses to rising  $\text{CO}_2$  and climate change—such as changes in stomatal conductance, transpiration, and leaf area—are already embedded in the CMIP6 Earth System Models used here<sup>54,55</sup>. These physiological effects are well documented to modify evapotranspiration and water fluxes, and thus are implicitly included in model-based  $\text{WY} = (\text{P} - \text{E})$  projections.

Consistent with our observational results, the model projections demonstrate that in drying regions, a 21% decrease in P (e.g., from  $\sim 500$  to  $\sim 400 \text{ mm}$ , as projected for the Mediterranean) is associated with an

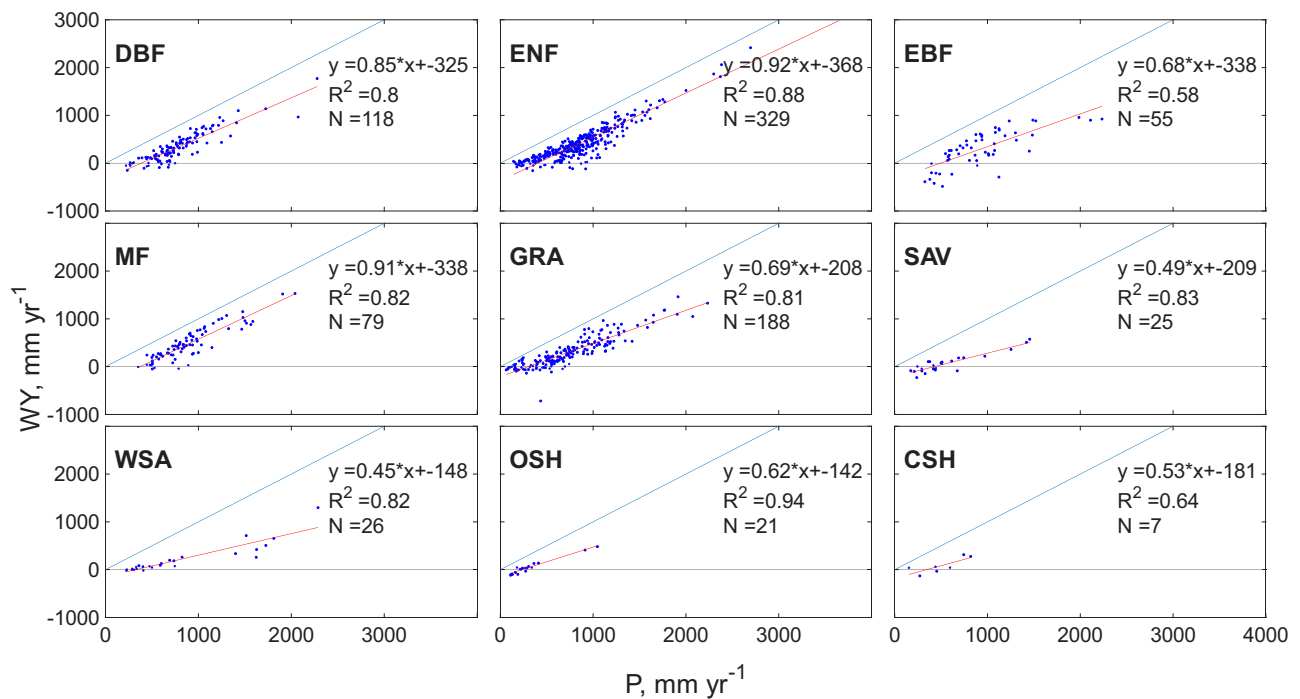


**Fig. 2 | Water yield response to precipitation by biome.** Variations in annual ecosystem water yield (WY) as a function of annual mean precipitation (P) across eddy covariance (EC) flux sites, grouped by biome type. Biome acronyms are

defined in Table S1; site data are summarized in Table S2. N indicates the number of data years available for each biome.

-87% decline in  $WY_{P-E}$  (Fig. 3)—a fourfold amplification. Conversely, a 21% increase in P (e.g., from -800 to -970 mm) yields a -44% increase in  $WY_{P-E}$ , a two-fold amplification. Across drying regions, the mean (negative) enhancement ratio ( $\Delta WY_{P-E}/\Delta P$ ) is 155%, compared with 112% in wetter regions. This asymmetric amplification resembles that observed in productivity responses<sup>51,56</sup>. While uncertainties remain in the magnitude of these responses across models, their incorporation reinforces our conclusion that WY is a sensitive, and amplifying, indicator of future climate projections.

Taken together, these results highlight that all water-budget terms matter, but WY has a particular advantage for climate change impact assessment. By combining integration across terms with amplified sensitivity, WY provides a powerful lens for identifying ecosystem thresholds, sustainability limits, and risks to water resources<sup>57</sup>.

Insights from site-scale evapotranspiration and water yield: The 56 sites that reported at least six years of evapotranspiration data with a sufficiently large range in precipitation (average  $P_{\max}/P_{\min} \sim 2.5$ ) permitted the analysis of water yield versus precipitation at the single site level. In some cases, paired sites with different vegetation types could also be used (Fig. 4, Table S2). Such higher resolution analysis revealed patterns similar to those observed at the larger biome scale, with large inter-annual variations in precipitation (e.g., a P range of -600 mm; Fig. 4A), but a conservative range of evapotranspiration values (ET range of -250 mm; Fig. 4A red data points), and a highly linear WY to P correlations in all sites ( $R^2 > 0.8$ ). Examining paired forest and non-forest ecosystems located in close proximity to each other demonstrates the impact of vegetation type on the sustainability limit (*i.e.*, on their  $P_{WY=0}$  value obtained from the equations in Fig. 4), which is as high as 551 mm in the forests but only 276 mm in the adjacent non-forest grassland site (Fig. 4B). These site-scale results highlight both the high sensitivity of water yield to decreases in precipitation and the significance of land cover type for sustainability. Such results also indicate the ecosystem ‘safety margin’, that is, the difference between the annual mean precipitation and the

$P_{WY=0}$  values. Such a safety margin demonstrates, first, the extent to which average evapotranspiration can be maintained as average precipitation declines while still permitting residual water yield ( $P > ET$ ). For example, the results in Fig. 4B (and the equations therein) indicate a safety margin of 195 mm for forest biomes (being the difference between mean  $P = 746$  and the local  $WY_{P=0} = 551 \text{ mm yr}^{-1}$ ). Second, it can be greatly extended to 470 mm in the grassland at the same location. Alternatively, ecosystem adjustments through tree mortality and reduced stand density can occur and will also improve water availability for societal needs.

In conclusion, we show that, for a given land cover and land use, ecosystem evapotranspiration values are surprisingly conservative. Evapotranspiration exhibits apparent saturation at a value below the energy limiting values and largely independent of climate and biome type. This inflexibility amplifies the sensitivity of water yield (WY) to precipitation variability, such that small changes in P lead to disproportionately large impacts on WY. This sensitivity is evident across observations and model projections with implications for increased flood risk in wetter regions and ecological collapse in drier zones. In such cases, land cover and water management must change<sup>2,7</sup>. Given its capacity to integrate both climatic forcing and biological regulation, WY should be adopted as an important indicator of hydrological sensitivity and ecosystem sustainability under climate change.

## Methods

### Data source

We obtained evapotranspiration (ET), precipitation (P), gross primary production (GPP) and related meteorological data from the EuroFlux (<http://gaia.agraria.unitus.it/home>), FLUXNET, AsiaFlux (<https://www.asiaflux.net/>), and AmeriFlux (<https://ameriflux.lbl.gov/>) databases of eddy covariance flux stations around the globe. We selected forest, grass, savanna, and shrub ecosystems, while excluding urban, agricultural, wetland, and water body sites, such that, of the 867 sites, 365 sites providing 2745 observation years were retained. For 162 of these sites, concurrent annual P and ET data were available for at least

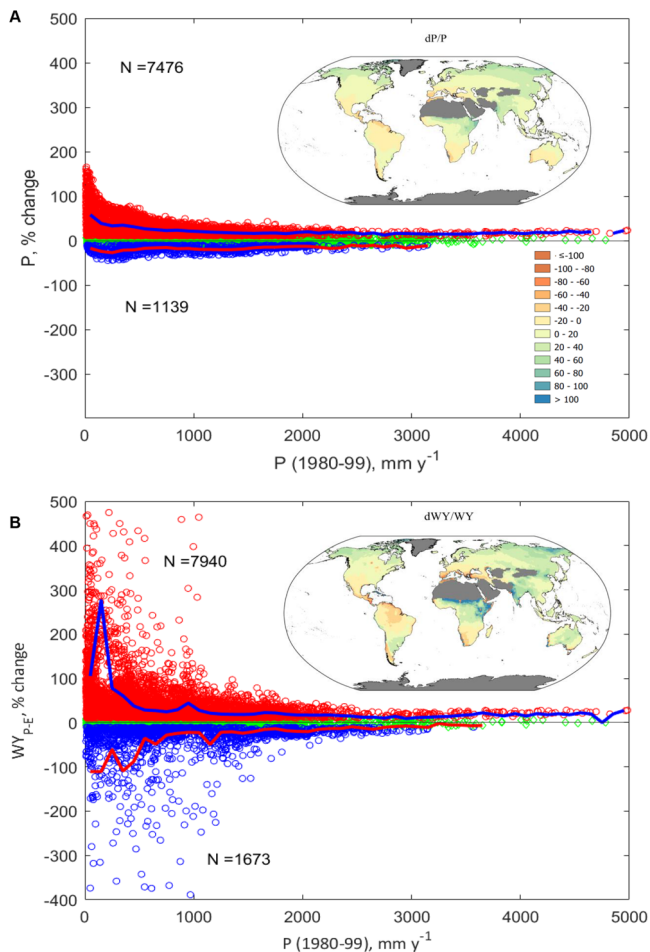


**Fig. 3 | Projected global changes in precipitation and enhanced water yield.** Projected (CMIP6; see “Methods”) changes in precipitation (P) and water yield (WY) over land, based on multi-model means for the periods 1980–1999 and 2080–2099 (denoted by subscripts 20 and 21, respectively). **A** Relative changes in precipitation are calculated as:  $\Delta P (\%) = (P_{21} - P_{20}) / P_{20} \times 100$ . **B** Relative changes in water yield ( $WY_{P-E}$ ) are computed as:  $\Delta WY (\%) = (WY_{21} - WY_{20}) / WY_{20} \times 100$ , where WY is approximated as  $P - E$ . Values are plotted against baseline  $P_{20}$ . Positive (red) and negative (blue) changes are shown separately for land areas within  $\pm 70^\circ$  latitude. Lines represent means within 100-mm precipitation bins. Green points ( $\pm 10\%$  change) are excluded from bin averaging. Inset maps show the spatial distribution of relative changes in  $\Delta P$  (panel **A**) and  $\Delta WY$  (panel **B**), illustrating that WY exhibits enhanced relative changes compared with P. Note: In some dry regions (e.g., the Sahel, Australia), even small reductions in P produce large relative changes in WY. In -1.7% of land grid cells, WY decreased despite increases in P, mainly in parts of Australia where evaporation was suppressed. The data were drawn using open-source application by QGIS Association, <http://www.qgis.org>.

one year, totaling 855 data years suitable for annual WY calculation. A summary of the data used, the source of the data, and available links to it are provided in Table S2 and S3. The main quality control algorithm used in the data preparation is described below. The sites used in the study provided a global coverage of most geographical and climatic zones (Fig. S8).

The dataset also includes 20 years of continuous flux measurements from the Yatir forest eddy covariance site<sup>17,58</sup> and seasonal measurements at two additional sites (Kadita and Biryá) along a natural rainfall gradient within Israel extended to an annual scale<sup>59,60</sup>, Table S4. The mean annual precipitation at these Two sites is 285 mm (Yatir), and 750 mm (Biryá and Kadita). Furthermore, of all sites (including forests, shrubs, and grasses) for which potential evapotranspiration (PET) can be calculated using the Food and Agriculture Organization’s Penman-

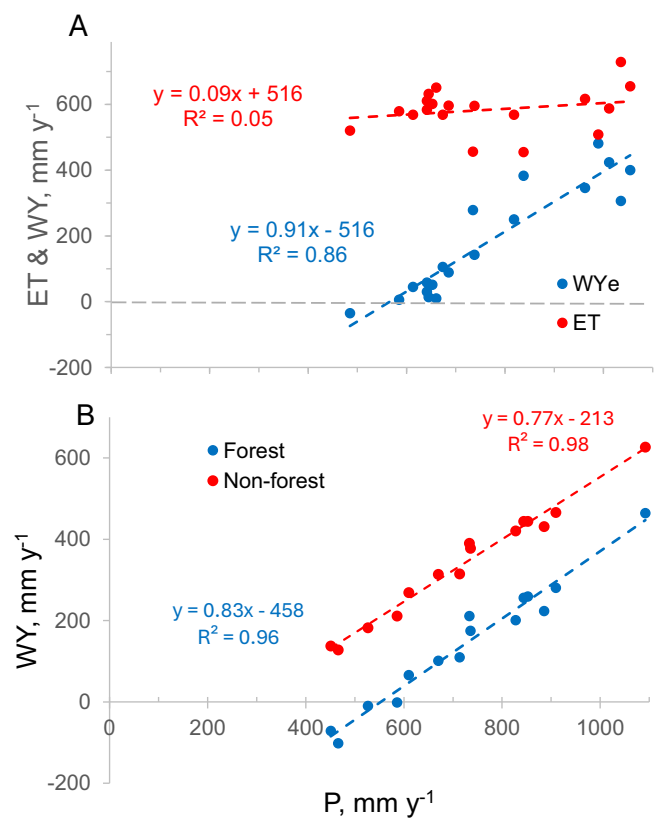


**Fig. 4 | Site-level contrasts in evapotranspiration and water yield.** **A** Multi-year average water yield (WY) at two paired ecosystem sites: a forest (ENF; Biryá) and an adjacent grassland (GRA; Kadita), both located in Israel (see the data in the Table S3). Despite having the same mean annual precipitation (P) of 746 mm, the mean ET differs substantially between the sites ( $545 \text{ mm yr}^{-1}$  for ENF and  $366 \text{ mm yr}^{-1}$  for GRA), resulting in distinct WY and  $P_{WY=0}$  values. **B** Comparison of multi-year annual evapotranspiration (ET; insensitive to P), and water yield (WY; high sensitivity to P) as a function of annual precipitation (P) at the Niwot Ridge evergreen needleleaf forest (ENF) site in the United States (mean P =  $800 \text{ mm yr}^{-1}$ ; mean ET =  $589 \text{ mm yr}^{-1}$ ). Site metadata for Niwot Ridge available at: <https://ameriflux.lbl.gov/sites/siteinfo/US-NRI>.

Monteith (FAO-PM) method, 107 (66%) are water-limited sites (i.e.,  $PET/P > 1$ ).

#### Data processing and quality control

Since the common temporal resolution between AmeriFlux, AsiaFlux, Euroflux, and FLUXNET sites was half-hourly steps, we based our analysis on this time step. As the databases usually include only data for latent heat of evaporation (LE;  $\text{Wm}^{-2}$ ) but not ET (water vapor flux,  $\text{mol m}^{-2}\text{s}^{-1}$ ), we first converted the half-hourly LE to ET using the equation  $ET = LE/\lambda$ , where  $\lambda$  is the specific heat of vaporization of water, and then calculated daily totals (for flux variables) and means (for meteorological variables). With regard to LE values obtained from the AmeriFlux network, gap-filled data were used when available (LE\_PIF variable, see <https://ameriflux.lbl.gov/data/aboutdata/data-variables/>) and, otherwise, primary LE data were used (LE variable). As data for different variables were frequently missing for some half hour periods within a day, the daily sum of half-hour periods ( $X_d$ ) for flux variables was calculated as  $X_d = \overline{X_{hh}} \cdot 48$ , where  $\overline{X_{hh}}$  is the mean value of half-hour periods for which variable X data were available, and 48 is the total number of half-hour periods in a day. Days missing more than eight half-hourly values of any variable were omitted from this variable to ensure data quality.

Annual sums (for flux variables) and means (for meteorological variables) were calculated similarly to daily values, keeping only data

from years with more than 300 available daily values recorded for each variable. Annual flux sums ( $X_y$ , where X is P, ET, or  $R_n$ ) were calculated similarly to daily totals, using  $X_y = \overline{X_d} \cdot N$ , where  $X_d$  is the annual daily average flux sum, and N is the number of days in the current year. We assumed that years for which there were data of any variable of interest covering at least 40 half-hourly periods daily on at least 300 days were representative of annual values for this variable.

For some Euroflux and FLUXNET-2015 database sites where the amount of data in half-hourly files was insufficient according to the quality control (QC) procedure described above but where the data in annual files for the variables of interest had a high ( $> 0.8$ ) QC level (the proportion of good data in a particular year, as provided by the site management team, see, e.g., FLUXNET2015 Variables Quick Start Guide, <https://fluxnet.org/data/fluxnet2015-dataset/variables-quick-start-guide/>), the data from annual files were used. As QC was performed for each variable separately, the number of annual values for different variables could differ.

The sites with high mean LE/ $R_n$  ratios were checked manually for possible errors in the data, and one site was excluded when yearly LE was higher than  $R_n$ . A dryland site at which  $ET > P$  was recorded consistently over a period of several years was also excluded, since this site was not a closed system, likely due to water supply from the water table.

### Data analysis

The dependencies between the variables under study were analyzed using linear and nonlinear regression. The effect of biome type on WY and related variables was analyzed using ANOVA. Data processing was performed using MATLAB 2023a software.

### CMIP6 models used in the water yield forecast

Monthly precipitation and evaporation were taken from 27 CMIP6 models<sup>53</sup> (listed below) under the 'r1i1p1f1' member. Specifically, we analyzed the historical experiment (integrated between the years 1850 and 2014) and the future Shared Socioeconomic Pathway 8.5 (SSP5-8.5) (through until year 2100).

The CMIP6 models (27) used for the simulation results reported here were: 'ACCESS-CM2', 'ACCESS-ESM1-5', 'AWI-CM-1-1-MR', 'BCC-CSM2-MR', 'CAMS-CSM1-0', 'CESM2', 'CESM2-WACCM', 'CMCC-CM2-SR5', 'CanESM5', 'EC-Earth3', 'EC-Earth3-Veg', 'FGOALS-f3-L', 'FGOALS-g3', 'FIO-ESM-2-0', 'GFDL-ESM4', 'INM-CM4-8', 'INM-CM5-0', 'IPSL-CM6A-LR', 'KACE-1-0-G', 'MIROC6', 'MPI-ESM1-2-HR', 'MPI-ESM1-2-LR', 'MRI-ESM2-0', 'NESM3', 'NorESM2-LM', 'NorESM2-MM', and 'TaiESM1'.

### Data availability

All the data reported in Figs. 1, 2 and 4B, as well as the summary of the data provided in Tables S1 and S2 are publicly available from the global networks' archives with the specific sites' locations (Table S2) and the relevant links and responsible PIs provided in Table S3. The data used in Figure 5B are from the study described in Ref. 59, and the data used in the figure provided in Table S4. CMIP6 data used in this paper are publicly available (Earth System Grid Federation (ESGF)) as described in Ref. 53. Figure 3 and S8 maps were prepared using open access application by QGIS Association, <http://www.qgis.org>.

### References

- Seneviratne, S. I. et al. Weather and Climate Extreme Events in a Changing Climate. In: *Climate Change 2021: The Physical Science Basis. Contribution of Working Group I to the Sixth Assessment Report of the Intergovernmental Panel on Climate Change* (ed Masson-Delmotte V., P. Zhai, A. Pirani, S. L. Connors, C. Péan, S. Berger, N. Caud, Y. Chen, L. Goldfarb, M. I. Gomis, M. Huang, K. Leitzell, E. Lonnoy, J. B. R. Matthews, T. K. Maycock, T. Waterfield, O. Yelekci, R. Yu, and B. Zhou). Cambridge University Press (2021).
- Caretta, M. A. et al. Water. In: *Climate Change 2022: Impacts, Adaptation and Vulnerability. Contribution of Working Group II to the Sixth Assessment Report of the Intergovernmental Panel on Climate Change* (ed H. O. Pörtner D. C. R., M. Tignor, E. S. Poloczanska, K. Mintenbeck, A. Alegría, M. Craig, S. Langsdorf, S. Lösschke, V. Möller, A. Okem, B. Rama). Cambridge University Press (2022).
- Yang, Y. T. et al. Evapotranspiration on a greening Earth. *Nat. Rev. Earth Environ.* **4**, 626–641 (2023).
- Oki, T. & Kanae, S. Global hydrological cycles and world water resources. *Science* **313**, 1068–1072 (2006).
- Zhang, K. et al. A global dataset of terrestrial evapotranspiration and soil moisture dynamics from 1982 to 2020. *Scientific Data* **11**, 445 (2024).
- Ellison, D., Futter, M. N. & Bishop, K. On the forest cover-water yield debate: from demand- to supply-side thinking. *Glob. Change Biol.* **18**, 806–820 (2012).
- Fisher, J. B. et al. The future of evapotranspiration: Global requirements for ecosystem functioning, carbon and climate feedbacks, agricultural management, and water resources. *Water Resour. Res.* **53**, 2618–2626 (2017).
- Bren, L., Lane, P. & McGuire, D. An empirical, comparative model of changes in annual water yield associated with pine plantations in southern Australia. *Aust. Forestry* **69**, 275–284 (2006).
- Albert, J. S. et al. Scientists' warning to humanity on the freshwater biodiversity crisis. *Ambio* **50**, 85–94 (2021).
- Yang, H., Xu, H., Huntingford, C., Ciais, P. & Piao, S. Strong direct and indirect influences of climate change on water yield confirmed by the Budyko framework. *Geogr. Sustainability* **2**, 281–287 (2021).
- Budyko, M. I. & Gerasimov, I. P. The heat and water-balance of the earth's surface, the general-theory of physical-geography and the problem of the transformation of nature. *Sov. Geogr. Rev. Transl.* **2**, 3–12 (1961).
- Zhang, L., Dawes, W. R. & Walker, G. R. Response of mean annual evapotranspiration to vegetation changes at catchment scale. *Water Resour. Res.* **37**, 701–708 (2001).
- Bosch, J. M. & Hewlett, J. D. A review of catchment experiments to determine the effect of vegetation changes on water yield and evapo-transpiration. *J. Hydrol.* **55**, 3–23 (1982).
- Williams, C. A. et al. Climate and vegetation controls on the surface water balance: Synthesis of evapotranspiration measured across a global network of flux towers. *Water Resources Res.* **48**, W06523 (2012).
- Baldocchi, D. Measuring fluxes of trace gases and energy between ecosystems and the atmosphere - the state and future of the eddy covariance method. *Glob. Change Biol.* **20**, 3600–3609 (2014).
- Kool, D. et al. A review of approaches for evapotranspiration partitioning. *Agric. Meteorol.* **184**, 56–70 (2014).
- Yaseef, R. az, Yakir, N., Rotenberg, D., Schiller, E. & Cohen, G. S. Ecohydrology of a semi-arid forest: partitioning among water balance components and its implications for predicted precipitation changes. *Ecohydrology* **3**, 143–154 (2010).
- Stoy, P. C. et al. Reviews and syntheses: Turning the challenges of partitioning ecosystem evaporation and transpiration into opportunities. *Biogeosciences* **16**, 3747–3775 (2019).
- Buckley, T. N. How do stomata respond to water status? *N. Phytologist* **224**, 21–36 (2019).
- Grossiord, C. et al. Plant responses to rising vapor pressure deficit. *N. Phytologist* **226**, 1550–1566 (2020).
- Massmann, A., Gentine, P. & Lin, C. J. When does vapor pressure deficit drive or reduce evapotranspiration? *J. Adv. Modeling Earth Syst.* **11**, 3305–3320 (2019).
- Novick, K. A. et al. The increasing importance of atmospheric demand for ecosystem water and carbon fluxes. *Nat. Clim. Change* **6**, 1023–1027 (2016).

23. Tenhunen, J. D., Lange, O. L., Gebel, J., Beyschlag, W. & Weber, J. A. Changes in photosynthetic capacity, carboxylation efficiency, and  $\text{CO}_2$  compensation point associated with midday stomatal closure and midday depression of net  $\text{CO}_2$  exchange of leaves of quercus-suber. *Planta* **162**, 193–203 (1984).
24. Banerjee, T. et al. Turbulent transport of energy across a forest and a semiarid shrubland. *Atmos. Chem. Phys.* **18**, 10025–10038 (2018).
25. Brugger, P. et al. Contrasting turbulent transport regimes explain cooling effect in a semi-arid forest compared to surrounding shrubland. *Agric. Meteorol.* **269**, 19–27 (2019).
26. Rotenberg, E. & Yakir, D. Distinct patterns of changes in surface energy budget associated with forestation in the semiarid region. *Glob. Change Biol.* **17**, 1536–1548 (2011).
27. Muller, J. D., Rotenberg, E., Tatarinov, F., Oz, I. & Yakir, D. Evidence for efficient nonevaporative leaf-to-air heat dissipation in a pine forest under drought conditions. *N. Phytologist* **232**, 2254–2266 (2021).
28. Muller J. D. et al. Detailed in situ leaf energy budget permits the assessment of leaf aerodynamic resistance as a key to enhance non-evaporative cooling under drought. *Plant Cell Environ.* **46**, 3128–3143 (2022).
29. Dusenge, M. E., Duarte, A. G. & Way, D. A. Plant carbon metabolism and climate change: elevated  $\text{CO}_2$  and temperature impacts on photosynthesis, photorespiration and respiration. *N. Phytologist* **221**, 32–49 (2019).
30. Yang, Y. T., Roderick, M. L., Zhang, S. L., McVicar, T. R. & Donohue, R. J. Hydrologic implications of vegetation response to elevated  $\text{CO}_2$  in climate projections. *Nat. Clim. Change* **9**, 44 (2019).
31. Asner, G. P., Scurlock, J. M. O. & Hicke, J. A. Global synthesis of leaf area index observations: implications for ecological and remote sensing studies. *Glob. Ecol. Biogeogr.* **12**, 191–205 (2003).
32. Xue, B.-L. et al. Global patterns, trends, and drivers of water use efficiency from 2000 to 2013. *Ecosphere* **6**, 10:174 (2015).
33. Chen, X. & Sivapalan, M. Hydrological basis of the Budyko curve: Data-guided exploration of the mediating role of soil moisture. *Water Resour.* **56**, 10 (2020).
34. Chen, Z. F., Wang, W. G., Cescatti, A. & Forzieri, G. Climate-driven vegetation greening further reduces water availability in drylands. *Glob. Change Biol.* **29**, 1628–1647 (2023).
35. Milly, P. C. D. Climate, soil-water storage, and the average annual water-balance. *Water Resour. Res.* **30**, 2143–2156 (1994).
36. Preisler, Y. et al. Mortality versus survival in drought-affected Aleppo pine forest depends on the extent of rock cover and soil stoniness. *Funct. Ecol.* **33**, 901–912 (2019).
37. Monteith, J. L. Evaporation and environment. In: *Symposia of the Society for Experimental Biology* (1965).
38. Priestley, C. H. B. & Taylor, R. J. On the Assessment of Surface Heat Flux and Evaporation Using Large-Scale Parameter. *Monthly weather Rev.* **100**, 81–92 (1971).
39. Cowan, I. R. & Farquhar, G. D. Stomatal function in relation to leaf metabolism and environment. *Symposium Society of Experimental Biology* **31**, 471–505 (1977).
40. Farquhar, G. D., Sharkey, T. D. & Ehleringer, J. R. A biochemical model of photosynthetic  $\text{CO}_2$  assimilation in leaves of  $\text{C}_3$  species. *Planta* **149**, 78–90 (1980).
41. Lloyd, J. & Farquhar, G. D. The  $\text{CO}_2$  dependence of photosynthesis, plant growth responses to elevated atmospheric  $\text{CO}_2$  concentrations and their interaction with soil nutrient status. *Funct. Plant Biol.* **23**, 915–925 (1996).
42. Medlyn, B. E. Reconciling the optimal and empirical approaches to modelling stomatal conductance. *Glob. Change Biol.* **17**, 2134–2144 (2011).
43. Still C. J. et al. No evidence of canopy-scale leaf thermoregulation to cool leaves below air temperature across a range of forest ecosystems. *Proc. Natl. Acad. Sci. USA* **119**, e2205682119 (2022).
44. Beer, C. et al. Temporal and among-site variability of inherent water use efficiency at the ecosystem level. *Global Biogeochemical Cycles* **23**, 1–13 (2009).
45. Gentine, P. et al. Coupling between the terrestrial carbon and water cycles—a review. *Environ. Res. Lett.* **14**, 8 (2019).
46. Cooley, S. S., Fisher, J. B. & Goldsmith, G. R. Convergence in water use efficiency within plant functional types across contrasting climates. *Nat. plants* **8**, 341–345 (2022).
47. Mauder, M., Foken, T. & Cuxart, J. Surface-Energy-Balance Closure over Land: A Review. *Bound. -Layer. Meteorol.* **177**, 395–426 (2020).
48. Mauder M., Jung M., Stoy P., Nelson J. & Wanner L. Energy balance closure at FLUXNET sites revisited. *Agric. Forest Meteorol.* **358**, 110235 (2024).
49. Dohn, J. et al. Tree effects on grass growth in savannas: Competition, facilitation and the stress-gradient hypothesis. *J. Ecol.* **101**, 202–209 (2013).
50. Zhang, M. F. et al. A global review on hydrological responses to forest change across multiple spatial scales: Importance of scale, climate, forest type and hydrological regime. *J. Hydrol.* **546**, 44–59 (2017).
51. Knapp, A. K., Ciais, P. & Smith, M. D. Reconciling inconsistencies in precipitation-productivity relationships: implications for climate change. *N. Phytologist* **214**, 41–47 (2017).
52. Fan, Y., Li, H. & Miguez-Macho, G. Global patterns of groundwater table depth. *Science* **339**, 940–943 (2013).
53. Eyring, V. et al. Overview of the coupled model intercomparison project phase 6 (CMIP6) experimental design and organization. *Geosci Model Dev.* **9**, 1937–1958 (2016).
54. Lemordant, L. & Gentine, P. Vegetation response to rising  $\text{CO}_2$  impacts extreme temperatures. *Geophys. Res. Lett.* **46**, 1383–1392 (2019).
55. Zarakas, C. M. et al. Plant physiology increases the magnitude and spread of the transient climate response to  $\text{CO}_2$  in CMIP6 earth system models. *J. Clim.* **33**, 8561–8578 (2019).
56. Huxman, T. E. et al. Convergence across biomes to a common rain-use efficiency. *Nature* **429**, 651–654 (2004).
57. Vicente-Serrano, S. M. et al. Evidence of increasing drought severity caused by temperature rise in southern Europe. *Environ. Res. Lett.* **9**, 044001 (2014).
58. Qubaja, R. et al. Partitioning evapotranspiration and its long-term evolution in a dry pine forest using measurement-based estimates of soil evaporation. *Agric. Forest Meteorol.* **281**, 107831 (2020).
59. Rohatyn, S. et al. Differential impacts of land use and precipitation on ‘ecosystem water yield’. *Water Resources Res.* **54**, 5475–5470 (2018).
60. Rohatyn, S. et al. Large variations in afforestation-related climate cooling and warming effects across short distances. *Commun. Earth Environ.* **4**, 18 (2023).

## Acknowledgements

We are grateful to Efrat Schwartz and Lior Segev for their assistance in the preparation of the data and figures. J.M. was supported by the Postdoc.Mobility stipend from the Swiss National Science Foundation, and by a fellowship from the Society of Swiss Friends of the Weizmann Institute. Josep Penuelas for useful comments on earlier version. This work was supported by funding from the Israel Science Foundation (ISF BRG grant 2481/22), and the KKL, and by the Institute for Environmental Sustainability (IES), the Kimmel and the de Bottom Centers at the Weizmann Institute of Science.

## Author contributions

The study was conceived by E.R. & D.Y.; E.R. and F.T. carried out the data analysis; J.M., E.R., F.T. & D.Y. analyzed the results and contributed to the writing.

## Competing interests

The authors declare no competing interests.

## Additional information

**Supplementary information** The online version contains supplementary material available at <https://doi.org/10.1038/s41467-025-66570-6>.

**Correspondence** and requests for materials should be addressed to Eyal Rotenberg or Dan Yakir.

**Peer review information** *Nature Communications* thanks David Schimel and the other, anonymous, reviewer(s) for their contribution to the peer review of this work. A peer review file is available.

**Reprints and permissions information** is available at <http://www.nature.com/reprints>

**Publisher's note** Springer Nature remains neutral with regard to jurisdictional claims in published maps and institutional affiliations.

**Open Access** This article is licensed under a Creative Commons Attribution-NonCommercial-NoDerivatives 4.0 International License, which permits any non-commercial use, sharing, distribution and reproduction in any medium or format, as long as you give appropriate credit to the original author(s) and the source, provide a link to the Creative Commons licence, and indicate if you modified the licensed material. You do not have permission under this licence to share adapted material derived from this article or parts of it. The images or other third party material in this article are included in the article's Creative Commons licence, unless indicated otherwise in a credit line to the material. If material is not included in the article's Creative Commons licence and your intended use is not permitted by statutory regulation or exceeds the permitted use, you will need to obtain permission directly from the copyright holder. To view a copy of this licence, visit <http://creativecommons.org/licenses/by-nc-nd/4.0/>.

© The Author(s) 2025